AFRL-SN-HS-TR- 2001- 002

X-BAND RADAR GROUND CLUTTER STATISTICS FOR RESOLUTION
CELLS OF ARBITRARY SIZE AND SHAPE

Mr. Bertus Weijers
Dr. James Ernstmeyer
Dr. Leon Poirier: ARCON Corporation
        260 Bear Hill Road
        Waltham MA 02154

January 1999 – October 1999

INHOUSE REPORT

APPROVED FOR PUBLIC RELEASE: DISTRIBUTION UNLIMITED

AIR FORCE RESEARCH LABORATORY
Sensors Directorate
80 Scott Dr
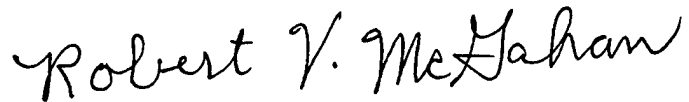**AIR FORCE MATERIEL COMMAND**
Hanscom AFB MA 01731-2909

IN HOUSE REPORT

Title: X-Band Radar Ground Clutter Statistics for Resolution Cells of Arbitrary
Size and Shape

PUBLICATION REVIEW

This report has been reviewed and is approved for publication:

APPROVED:

Robert V. McGahan

ROBERT V. McGAHAN
Technical Advisor
Electronics Technology Division

APPROVED/DISAPPROVED.

Richard Payne

RICHARD PAYNE
Division Chief
Electromagnetics Technology Division
AFRL/SNH

REPORT DOCUMENTATION PAGE

Form Approved
OMB No. 0704-0188

1. REPORT DATE *(DD-MM-YYYY)*	2. REPORT TYPE	3. DATES COVERED *(From - To)*
	In House	Jan 1999 - Oct 1999

4. TITLE AND SUBTITLE
X-Band Radar Ground Clutter Statistics for Resolution Cells of Arbitrary Size and Shape

5a. CONTRACT NUMBER

5b. GRANT NUMBER

5c. PROGRAM ELEMENT NUMBER
62702F

6. AUTHOR(S)
Ernstmeyer, James
Weijers, Bertus
Poirier, Leon

5d. PROJECT NUMBER
4600

5e. TASK NUMBER
15

5f. WORK UNIT NUMBER
46001514

7. PERFORMING ORGANIZATION NAME(S) AND ADDRESS(ES)
1. Air Force Research Laboratory
   Sensors Directorate
   Hanscom AFB MA 01731
2. ARCON Corporation
   260 Bear Hill Road
   Waltham, MA 02154

8. PERFORMING ORGANIZATION REPORT NUMBER

9. SPONSORING/MONITORING AGENCY NAME(S) AND ADDRESS(ES)

10. SPONSOR/MONITOR'S ACRONYM(S)

11. SPONSOR/MONITOR'S REPORT
AFRL-SN-HS-TR-2001-002

12. DISTRIBUTION/AVAILABILITY STATEMENT
APPROVED FOR PUBLIC RELEASE: DISTRIBUTION UNLIMITED.   ESC-01-0154

13. SUPPLEMENTARY NOTES

14. ABSTRACT
A procedure is developed for predicting the clutter reflectivity and probability density function of X-band radar clutter returns for resolution cells of arbitrary size and shape. The prediction uses high-resolution measurements of phase and amplitude of the ground reflections made by synthetic aperture radar (SAR) to estimate the properties of the clutter that would be observed with lower resolution radars. Clutter scene images collected by the MSTAR Program form the basis of this work.

MSTAR public clutter scene data consists of spotlight mode X-band SAR images with typical resolution 0.3 x 0.3 m. Under certain assumptions, the statistics of the image pixels will approximate those of the associated clutter cells. The probability distribution of the complex pixel amplitudes is found to be significantly non-Gaussian. Larger resolution cells are constructed by coherently combining the returns from adjacent pixels. The statistical properties of clutter in these larger resolution cells is examined for a variety of cell sizes, shapes, and underlying terrain types.

15. SUBJECT TERMS
Radar Clutter Statistics, SAR Clutter

16. SECURITY CLASSIFICATION OF:			17. LIMITATION OF ABSTRACT	18. NUMBER OF PAGES	19a. NAME OF RESPONSIBLE PERSON
a. REPORT	b. ABSTRACT	c. THIS PAGE			Bertus Weijers
UNCLAS	UNCLAS	UNCLAS	UNC		19b. TELEPHONE NUMBER *(Include area code)* (781) 377-2527

Standard Form 298 (Rev. 8/98)
Prescribed by ANSI Std. Z39.18

CONTENTS

FIGURES

TABLES

1. Introduction

There are several motivations for this work. First, airborne and space-based radars must detect targets against a background of interfering reflections from the earth's surface that fluctuate randomly in both time and space. In order to optimize the detection performance of a radar system in the presence of clutter, its intensity and statistical behavior must be known and accounted for.[1] Knowledge of the intensity and statistics of clutter is critical to the design of both airborne and space-based radar.

Second, we are motivated by the recent emphasis on space-based radar designs incorporating distributed aperture antennas, exemplified by the TechSat 21 experimental radar system.[2] Their two-way antenna patterns are vastly more complicated than the main beam and sidelobes of a single aperture. The patterns contain many tens of grating lobes of roughly equal peak amplitude, which may or may not be sharply defined or regularly spaced. Moreover, the patterns change continually throughout an orbit. The essentially infinite variety of unconventional antenna patterns presented by such systems lead us to seek a means to simulate the effects of arbitrary antenna patterns.

Third, even though clutter often limits radar performance, measured clutter data is available only for limited grazing angles and terrain types. This is because of the high cost of instrumenting well-calibrated clutter measurement radars and the difficulty of deploying the radars over the needed ranges of grazing angle and terrain types. The applicability of available clutter prediction codes is also limited. For example, they do not predict accurately the clutter reflectivity at low grazing angles where shadowing and multiple scattering become important. This region makes up a substantial fraction of the coverage area required of airborne and space-based radars.

For these reasons we took advantage of the high-resolution MSTAR SAR data to estimate the clutter that would be experienced by lower resolution airborne and space-based surveillance radars.[3]

---

[1] Skolnik, M. I. (1980) *Introduction to Radar Systems, 2 ed.*, McGraw-Hill, New York, 485-496.
[2] TechSat 21, Sparse Array Workshop, Air Force Research Laboratory, Space Vehicles Directorate, Kirtland AFB, NM, 28-29 July 1998
[3] MSTAR (Public) Clutter, Web: http://www.mvblab.wpath.af.mil/public/MBVDATA; E-mail: cdhelp@mvblab.wpafb.af.mil; FAX: 937-656-4412

2. Characterizing Clutter

The antenna pattern, in conjunction with the radar signal bandwidth, dictates the shape and size of the clutter resolution cell. The clutter resolution cell is that portion of the antenna pattern footprint that is simultaneously illuminated by all range-ambiguous pulses of transmitted radar energy. The resolution cell reflects the complicated spatial structure exhibited by the antenna pattern. This fact is illustrated in Figure 1, which shows a calculated antenna pattern and resolution cell consistent with TechSat 21 radar parameters.

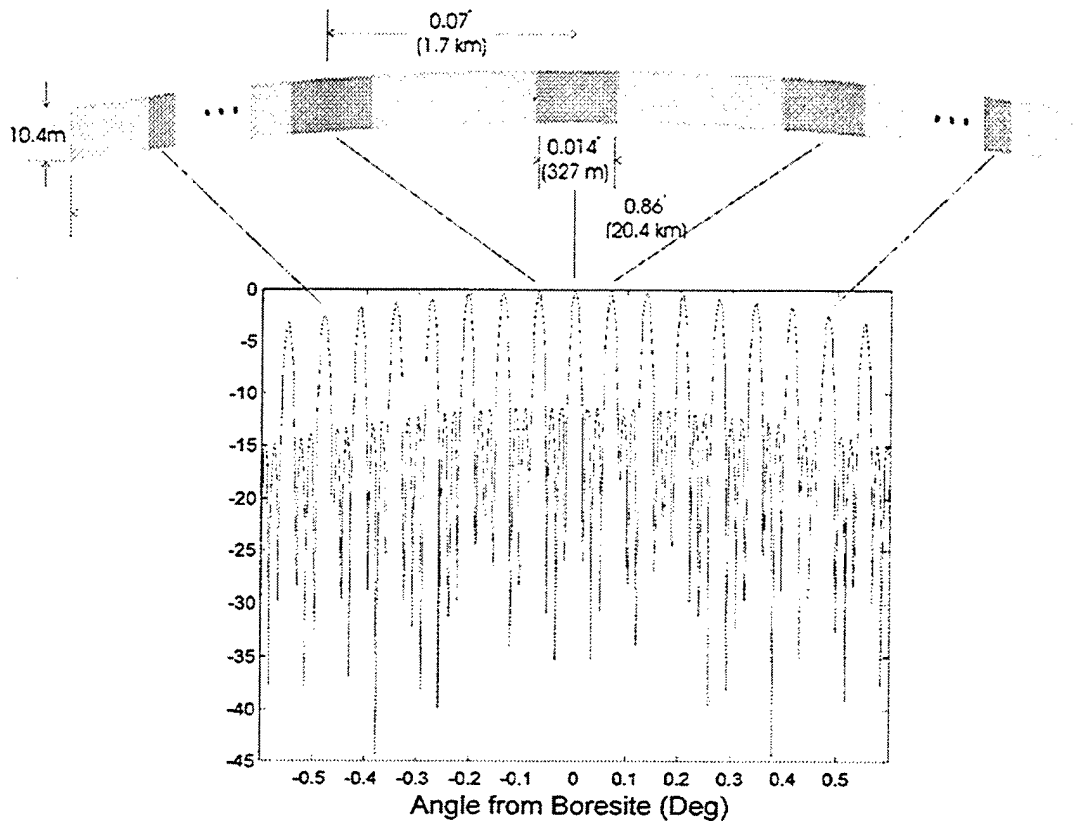Figure 1. TechSat 21 Radar Footprint. Radar is located over the bottom of the page, illuminating the footprint shown at a slant range of 1300 km. Calculation assumes a 3 element by 6 element array, spaced at 25 m, with uniform illumination. Each element is a 2.4 m diameter phased array antenna, with 40 dB Taylor weighted illumination across its aperture. Duration of the transmitted pulses is 50 ns.

The clutter resolution cell dimensions determine the received clutter intensity and affect its statistical distribution, thereby influencing radar performance. It is well-known that the variance of radar ground and sea clutter returns tends to increase as the surface area illuminated by radar decreases.[4,5]. This implies a change in the underlying clutter statistical distribution, accompanied by the above-noted effects on radar performance. Thus, the peculiarities of the exotic and highly variable antenna pattern of the distributed aperture radar may impact the statistics of the received clutter, and thereby radar performance. Because of this interdependence, the distributed aperture radar will face performance challenges that have never before been addressed. It is the purpose of this work to develop a procedure for predicting the mean normalized intensity and fluctuation statistics associated with an arbitrary antenna footprint.

A number of different statistical distributions have been used to model the fluctuating returns associated with radar clutter. Among these are the Rayleigh, log-normal, and Weibull distributions.[1] The Rayleigh distribution may be considered benign in the sense that large magnitude clutter returns occur with relatively low probability. By the same token, log-normal clutter is severe, while Weibull is intermediate between the two. The choice of statistical model depends on the characteristics of the underlying terrain. In this work, the Rayleigh and log-normal distribution will be used as benchmarks to which data will be compared.

Several researchers have successfully used the Gaussian probability density function (pdf) to model the statistical distribution of the radar receiver voltage produced by clutter returns from desert, farmland, and the sea surface in cases where the sea wavelength is short compared to a radar resolution cell.[6] Clutter which generates receiver voltages obeying a Gaussian pdf is known as Rayleigh clutter. The pdf for a zero-mean, Gaussian random variable, X, representing either the in-phase (I) or quadrature (Q) component of the complex receiver voltage, is given in Eq. (1).

$$f_X(v) = \frac{1}{\sigma\sqrt{2\pi}} \exp\left(-\frac{v^2}{2\sigma^2}\right) \tag{1}$$

This distribution is parameterized only by the variance, σ^2.

Starting with the Gaussian model for the statistical behavior of the receiver voltages, I and Q, it is straightforward to derive the corresponding models for the complex envelope, or amplitude of the received signal, and for the received power or intensity. Together, these models for the statistics of the receiver voltages, complex envelope, and power, all derived from Gaussian receiver voltages, are known as Rayleigh clutter statistics. From a fundamental perspective, the Rayleigh model accurately describes reality when the clutter source comprises a large number of scatterers producing roughly equal amplitude returns.

[4] Ulaby, F. T., Moore, R. K., and Fung, A. K. (1986) *Microwave Remote Sensing, Active and Passive, Volume II*, Artech House, Norwood, MA, 903

[5] Fung, Adrian K., (1990) *Effect Of Cell Size On Radar Clutter Statistics*, University of Texas at Arlington, RADC Tech. Rpt. RADC-TR-90-235

[6] Andrews, G. A. and Gerlach, K. (1989), "SBR Clutter and Interference", in *Space-Based Radar Handbook*, L.J. Cantafio, ed., Artech House, Norwood, MA, 388.

The Rayleigh model for the receiver voltage amplitude is the square root of the sum of two squared Gaussian random variables of equal variance, $A = \sqrt{I^2 + Q^2}$. The resulting random variable has a chi-distribution with two degrees of freedom.[7] Its pdf is given by:

$$f_A(V) = \begin{cases} \dfrac{V}{\sigma^2} \exp\left(-\dfrac{V^2}{2\sigma^2}\right); & V \geq 0 \\ 0; & V < 0 \end{cases} \qquad (2)$$

where σ^2 remains the variance of either of the quadrature voltages. The distribution described by Eq. (2) is also called the Rayleigh pdf.

Finally, the Rayleigh model for received power is proportional to the sum of the squares of two Gaussian random variables, or equivalently, proportional to the square of the random variable, V. The resulting random variable, $P = \alpha V^2$, is known as a chi-square with two degrees of freedom, having a pdf given by:

$$f_P(p) = \begin{cases} \dfrac{1}{2\alpha\sigma^2} \exp\left(-\dfrac{p}{2\alpha\sigma^2}\right); & p \geq 0 \\ 0; & p < 0 \end{cases} \qquad (3)$$

Equivalently, the power is distributed according to an exponential pdf, (Eq. 4) with mean $\overline{P} = 2\alpha\sigma^2$.

$$f_P(p_c) = \begin{cases} \dfrac{1}{\overline{P}} \exp\left(-\dfrac{p_c}{\overline{P}}\right); & p_c \geq 0 \\ 0; & p_c < 0 \end{cases} \qquad (4)$$

An alternative pdf, the log-normal, has been found to approximate the observed statistical distribution of receiver power returned from mountainous terrain, urban areas, and rural scenes containing large discrete scatterers such as buildings and silos.[1] These clutter scenes share the property that only a few dominant scatterers are contained in each clutter resolution cell. The log-normal pdf is given by:

$$f_P(p_c) = \begin{cases} \dfrac{1}{\sqrt{2\pi}\, p p_c} \exp\left[-\dfrac{1}{2p^2}\left(\ln\dfrac{p_c}{p_m}\right)^2\right]; & p_c \geq 0 \\ 0; & p_c < 0 \end{cases} \qquad (5)$$

where p is the standard deviation of $\ln p_c$, and p_m is the median value of p_c.

---

[7] Papoulis, A. (1965) *Probability, Random Variables, and Stochastic Processes*, McGraw-Hill, New York, 250-266.

Figure 2 compares the shapes of the power distributions for Rayleigh and log-normal clutter. The two distributions are calculated to have the same mean clutter value. The figure illustrates the higher probability of realizing large clutter power in the log-normal case than in the Rayleigh case. Because of this property the log-normal distribution is often referred to as having "higher tails."
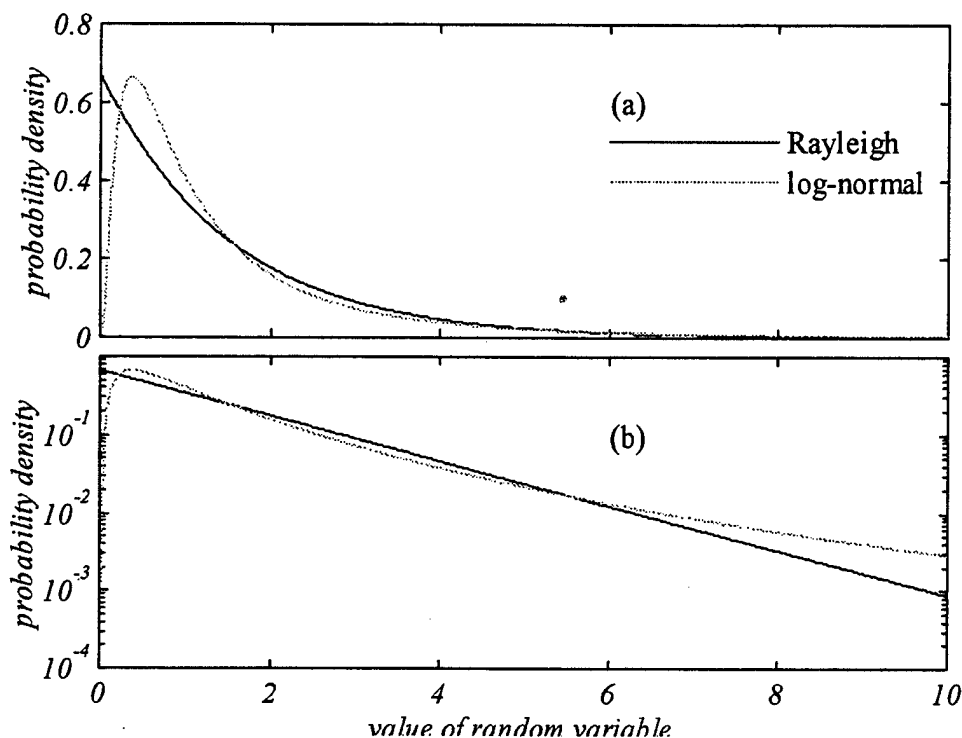
Figure 2: Comparison Between Rayleigh And Log-Normal Probability Density Functions. Mean of the distribution is the same for both cases. (a) Linear scale and (b) logarithmic scale plots of the same data illustrate that a Rayleigh random variable will realize low values with greater likelihood than a log-normal random variable. The log-normal random variable has a relatively higher probability of realizing large values, as seen from the higher "tail" of the log-normal pdf in (b).

The exponential (Rayleigh) and log-normal models for clutter power given in Eq. (4) and Eq. (5) are the benchmarks with which actual, observed clutter distributions will be compared in this report. They are chosen because they exemplify the extreme cases of high tails and low tails on the clutter distribution. In addition, we will show that both of these distributions provide good fits to the MSTAR clutter fluctuation data under appropriate conditions.

3. Constructing the Reflectivity for an Arbitrary Clutter Cell

The data obtained from the spotlight SAR mode MSTAR airborne radar provides well-calibrated values of high-resolution (0.3 x 0.3 m) clutter samples for a range of

grazing angles and several homogeneous and non-homogeneous terrain types.[*] We analyzed the fluctuation statistics and determined the mean normalized radar reflectivity from the recorded complex voltages of the pixels/cells that make up the image/footprint. To characterize the clutter observed by a lower resolution non-imaging radar, we added the contributions (complex pixel voltages) of the neighboring high-resolution cells that fill the clutter cell of the lower resolution radar.

Our starting point is the measured high-resolution complex clutter scene reflectivity $g(x_i, y_i)$ of the range-angle resolution cell sample of the ground at the indexed ground position (x_i, y_I). The radar cross section of a resolution cell of area a is $\sigma_{Ci} = |g(x_i, y_i)|^2 a$. The $g(x_i, y_i)$ are obtained from the processed output of the synthetic aperture radar system. The output value for each pixel/cell of the SAR image is proportional to the complex receiver voltage generated by the scatterers in that cell/pixel. Thus, $g(x_i, y_i)$ represents an amplitude reflectivity in meters per meter, instead of a power reflectivity, which would be proportional to the normalized radar cross section σ_o of the resolution cell in square meters per square meter.

An estimate of the reflectivity for the same terrain and grazing angle appropriate for a lower-resolution radar is obtained by adding the high-resolution complex reflectivities $g(x_i, y_i)$ of the cells that span the new clutter cell. Thus, the clutter reflectivity G of a cell of arbitrary size and shape is

$$G = \sqrt{\frac{a}{A}} e^{j2kr} \sum_{i=1}^{N} g(x_i, y_i) e^{-j2kr_i}, \qquad (6)$$

where a and A are the small- and large-cell areas, respectively, k is the wavenumber, N the number of small cells in the new large cell, r the slant range to the new cell, and r_i the slant ranges to each of the small cells. In writing Eq. (6) we assumed that there is no significant interaction between adjacent high-resolution cells and that the scattering amplitudes of the individual scatterers in each cell do not change significantly over the bandwidths in question.

After SAR processing, a coherent summation of the returns from multiple pixels (as specified by Eq. (6)) is equivalent to a coherent summation of the returns from the scatterers in those pixels provided that there is no significant interaction among neighboring cells.[8]

During the course of SAR processing, returns from scatterers everywhere within the extent of the footprint of the real aperture of the SAR antenna contribute to each of the image pixel amplitudes. We examine in broad terms the technique used to produce a SAR image. The complex receiver voltage V_{mn}, at time t_n (or range gate n), and from pulse m, is the sum of the contributions from all of the scatterers, indexed by k, in the range gate n of the real aperture footprint.

---

[*] The data were actually recorded as a function of depression angle. However, in this report, we use the grazing angle that we assumed to be equal to the depression angle.
[8] Skinner, J. Paul, Kent, Brian M., Wittman, Ronald C., Mensa, Dean L. and Andersh, Dennis J. "Normalization and Interpretation of Radar Images, IEEE Trans. AP VOL. 46, No. 4, April 1998

$$V_{mn} \propto \sum_{k} A_{kn} e^{j\theta_{kn}} e^{jR_m(x_k, y_k)} e^{\phi(t_n)}, \tag{7}$$

where $A_{kn} e^{j\theta_{kn}}$ is the amplitude and phase associated with the kth scatterer in range gate n, (x_k, y_k) is the position of the kth scatterer, $R_m(x_k, y_k)$ is the round trip phase path between the kth scatterer and the antenna location at the time of pulse m, and $\phi(t_n)$ is the phase associated with the linear FM chirp of the transmitted pulse. The first step in image reconstruction for the case of a spotlight mode SAR system is to perform a polar-to-Cartesian interpolation. The interpolation technique employed can be quite nonlinear as a function of position, but will always be a linear transformation of the receiver voltages V_{mn}:

$$V'_{rs} = \sum_{m,n} B_{rsmn} V_{mn}, \tag{8}$$

where V'_{rs} are the Cartesian grid voltages and B_{rsmn} are real coefficients. If it were necessary to window the data for the purpose of reducing sidelobes, this could be accomplished by a separate linear transformation of the Cartesian grid voltages. Equivalently, the coefficients in Eq. (8) could be replaced by the inner product between B_{rsmn} and the windowing transformation—accomplishing the same result in a single step identical in appearance to Eq. (8). Thus, we can omit the windowing step without loss of generality. Likewise, we omit the transformation from the slant plane to the ground plane. We can therefore view Eq. (8) as an expression that takes in the polar raster receiver voltages, V_{mn}, and produces the corresponding voltages, V'_{rs}, that have been interpolated onto a Cartesian grid, windowed, and projected onto the ground plane. Finally, the pixel value of the reconstructed image, v_{pq}, is obtained as the inverse, two-dimensional, discrete Fourier transform[9] of the V'_{rs}:

$$v_{pq} = \frac{1}{RS} \sum_{r=0}^{R-1} \sum_{s=0}^{S-1} V'_{rs} e^{-2\pi j rp/P} e^{-2\pi j sq/Q}, \tag{9}$$

where R is the total number of pulses, and S is the total number of range gates, or samples in time, for each pulse. The value of g_{pq} is precisely the complex voltage associated with the pth pixel in cross-range, and the qth pixel in range.

Using Eqs. (7) and (8) in Eq. (9), we can rewrite the reconstructed image as

$$g_{pq} = \frac{1}{RS} \sum_{k} \sum_{r=0}^{R-1} \sum_{s=0}^{S-1} \sum_{mn} A_{kn} e^{j\theta_{kn}} B_{rsmn} e^{-2\pi j rp/P} e^{-2\pi j sq/Q} e^{jR_m(x_k, y_k)} e^{\phi(t_n)} \tag{10}$$

---

[9] Jakowatz, C. V., Wahl, D. E., Eichel, P. H., Ghiglia, D. C., and Thompson, P. A. (1996) Spotlight-Mode Synthetic Aperture Radar: A Signal Processing Approach, Kluwer Academic Publishers, Boston, 107-109.

From Eq. (10) we see that the image is ultimately just a linear combination of the individual complex scatterer amplitudes. The weighting applied to these amplitudes yields precisely the effective azimuth antenna pattern and the compressed pulse range resolution of the synthetic aperture radar. For the simple special case of uniform weighting, the processing maps out a 2-dimensional sinc function in (x_k, y_k) for a given pixel p,q.[9] Thus, scatterers located within the resolution cell of the SAR, in the main lobe of the sinc function, are weighted much more heavily than scatterers elsewhere in the physical domain of the image. The disparity in weighting between the main lobe and elsewhere would be even greater if a tapered window were used to reduce sidelobes. Thus, the image pixel values are dominated by the scatterers contained in the corresponding physical ground cells. In the case of the MSTAR SAR system, the size of the resolution cell is quite small (0.3 m square), so that only a few scatterers will dominate each pixel return.

The salient point in this discussion is that when we coherently add the clutter returns in a group of adjacent pixels, as proposed in Eq. (6), we are in fact coherently adding the contributions of all the scatterers contained in the large patch of terrain imaged by the pixels in question. Scatterers outside that patch do not contribute. This is fundamentally the same situation as if the patch were the clutter cell of a lower resolution radar.

It should be pointed out that in the case of a high resolution SAR system the weighting of Eq. (10) singles out a small number of scatterers. We should, therefore, not expect the statistical behavior of the real and imaginary pixel voltages to be Gaussian, as has been suggested by other authors.[10] They argue that the samples of complex receiver voltage, V_{mn}, represent sums of contributions from a large number of independent scatterers and so, from the Central Limit Theorem (CLT)[7], should exhibit Gaussian distributions. This is certainly a reasonable conclusion, since the conditions of the CLT are satisfied in Eq. (7). Namely, there are a large number of scatterers (hundreds); the contributions of the scatterers are statistically independent; the statistical distribution of each individual contribution has a finite higher moment greater than 2; and all of the contributions have comparable variance, in the sense that:

$$\lim_{K \to \infty} \sum_{k=1}^{K} \text{var}\left[A_k e^{j\theta_k} e^{jR_m(x_k, y_k)} e^{\phi(t_n)} \right] = \infty. \tag{11}$$

However, they go on to argue that the image pixel values represent a linear combination of the independent Gaussian random variables V_{mn}, and that they are therefore Gaussian themselves.[7] This reasoning is fallacious because the V_{mn} are not independent. In fact, Eq. (7) shows them to be highly correlated combinations of the same physical variables. Moreover, Eq. (10) demonstrates that the pixel values incorporate contributions from only a small number of scatterers in the case of small resolution cells. This fact violates

---

[10] Curlander, J. C. and McDonough, R. N. (1991) Synthetic Aperture Radar: Systems and Signal Processing, John Wiley & Sons, New York, 215.

the assumptions of the CLT, Eq. (11) in particular, so that we should not expect the statistical distribution of the pixel values to be Gaussian. Rather, the pixel statistics will reflect the statistics of the contributing scatterers.

Several additional assumptions underlie the proposed approach of constructing the clutter return from an arbitrary resolution cell using pixel values according to Eq. (6). First, the SAR imaging time must be short enough that the scene is stationary during image formation. This requirement stems from the fact that we treat $A_k e^{j\theta_k} e^{jR_m(x_k, y_k)}$ as a temporal constant in (9) and in subsequent calculations. If the scatterers themselves, $A_k e^{j\theta_k}$, or their positions, (x_k, y_k), are changing during the imaging time, then the sums over pulses and scatterers in Eq. (10) will in fact be sums over temporal variation as well. The resulting image will then not be characteristic of the scatterers at a given point in time, but instead be a weighted average in time. The requirement of scene stationarity places a limit on the amount of wind-induced motion that can be tolerated during image formation. This motion can at most be a small fraction of the radar wavelength. Certainly this assumption will be satisfied in the limit of a calm day or sufficiently short imaging time. In the case of the MSTAR data collections, the 6 s typical imaging time limits the strict applicability of this approach to low wind conditions.

Second, to use the SAR data in the manner proposed here, the SAR system angular diversity must be small relative to the aspect angle dependence of the scene. For spotlight mode SAR, the viewing angle presented by individual scatterers will vary over an interval equal to the angular diversity of the system. If the back-scattered return from a cell is not aspect angle independent, an extraneous, pulse-to-pulse variation in scatterer amplitude and phase is introduced in Eq. (7). Such conditions invalidate the procedure by preventing the image reconstruction algorithm from fully attenuating out-of-cell scattering contributions. Large man-made metallic objects in the clutter scene present the greatest problem. They are composed of smooth surfaces and facets that produce large specular reflections, rapid fluctuations in scattering return over a fine angular scale and large interaction between adjacent cells.[8,11] Because of this possibility, we limit consideration only to clutter scenes free of man-made metallic targets. Moreover, the angular diversity of the MSTAR data collections used in this work is 4°, and we assume that the radar cross section of the foliage cover does not change significantly over this narrow angular range.

In the case that multiple, unresolved scatterers are present in a SAR pixel, the observed complex pixel amplitude is the result of interference of two or more scattered signals. The resultant pixel amplitude will then change as a function of the viewing angle from the radar platform to the pixel. The worst case variation is experienced when the scatterers are separated by the full pixel dimension, approximately 10 wavelengths. Then, the width of the main scattering lobe is about 5°, a little wider than the angle diversity of the SAR.

Another concern arising from the present approach is that in order to change the range dimension of a resolution cell, a radar must change its bandwidth, whereas here we claim the same effect by the algebraic manipulation of data from a fixed bandwidth system. The fixed bandwidth of the SAR system is very wide, namely a 500 MHz linear FM sweep. This is much greater than the bandwidth of any surveillance radar system and

---

[11] Skolnik, M. I. (1980) *Introduction to Radar Systems*, 2 ed., McGraw-Hill, New York, 40.

9

we assume that the scattering amplitudes of individual scatterers are independent of frequency over the bandwidth of the high-resolution SAR. Changing the radar frequency will change the phase path length between scatterers located in the same pixel. In the worst case, a 500 MHz sweep at X-band leads to full wavelength of phase path change over the range dimension of the pixel. This will give rise to a different realization of each of the clutter pixels. Since the size and orientation of the surface patch associated with each pixel has not changed, we would not expect the statistical distribution of the observed clutter to change—only the individual realizations have been altered.

4. MSTAR Clutter Scene Data

The MSTAR data collection of September 1995 forms the basis of the work presented here. The collection was performed by the Sandia National Laboratory in the vicinity of Huntsville, Alabama. It was provided to the authors courtesy of the Target Signature Branch, Air Force Research Laboratory.[3]

The data consist of spotlight-mode synthetic aperture radar images taken from a Twin Otter aircraft flying 55.4 m s^{-1} at an altitude of approximately 1360 m. The images were collected over an angular range of ± 2.28° about broadside. The aperture time was 6.23 s, yielding a synthetic aperture length of 345 m. The images examined here were collected at approximately 0830 hours Central Time, 5 September 1995. Images taken at grazing angles $\psi = 15°, 30°$, and 45° are available in the 1995 data collection, but this report will focus on the 15° data.

The MSTAR data files provide both amplitude and phase information for each pixel in the image. The data has not been processed to remove speckle. Calibration factors included in each file allow the pixel magnitudes to be calculated absolutely as the square root of the resolution cell radar cross section. Pixel magnitudes are thus measured in units of meters. The complex pixel value determined by the magnitude and phase associated with each pixel is proportional to the receiver voltage contribution produced by that pixel.

The normalized clutter reflectivity, σ_c, associated with each pixel is obtained by squaring the pixel value and dividing by the ground-projected area of the clutter resolution cell.

$$\sigma_C = \frac{\cos\psi}{\Delta R\Delta C}\left|v_{pq}\right|^2 \tag{12}$$

where ψ is the grazing angle at the clutter patch and v_{pq} is the complex pixel value. The cell area is $a = \Delta R\Delta C/\cos\psi$ where ΔR is the range resolution and ΔC is the cross range resolution. The normalized radar clutter cross section, known commonly as σ_o is the mean value of many independent realizations of σ_o.

Figure 3 shows a typical intensity image from the MSTAR clutter scene data set. The antenna aim point is 34.8° N latitude, 86.8° W longitude, and is viewed at a 15° depression angle from the aircraft. The range and cross-range resolution of the image is 0.305 m, with 1784 pixels in range and 1476 pixels in cross-range. The scene is

oversampled to produce range and cross-range pixel spacings of 0.202 m and 0.203 m, respectively. The dimensions of the physical domain captured in the image are 350 m in range by 300 m in cross-range. The other images presented in this report share the same size, resolution, and pixel spacing.

Figure 3 shows terrain that is typical of the entire data set, namely, a rural environment combining forest and cropland. The aircraft is located beyond the bottom of the image, at a range of 4500 m. The wide black bands are radar shadows cast by the 15 - 18 m tall trees located in the areas of the image exhibiting high relief. The flat areas are cultivated land. The linear feature extending horizontally across the bottom of the image is a farm road.

Figure 3. Typical MSTAR Clutter Scene. Intensity image of mixed forest and cropland about an aim point located at 34.8° N latitude, 86.8° W longitude, and viewed at a 14.8° grazing angle. Radar aircraft is located at bottom of page. Dark bands are radar shadows.

While the clutter scene shown in Figure 3 is useful for illustrating the features present in the other images we will analyze, it is not well-suited to studying the statistical behavior of the clutter pixels or of the constructed clutter cells. For that purpose we seek images of homogeneous terrain and foliage cover. An homogeneous image allows us to obtain a large number of independent spatial realizations of the same terrain type. Such an ensemble of equivalent realizations is necessary to estimate the statistical distribution

of the clutter returns that characterize a particular terrain type. In this report, we will focus on flat terrain with two alternative foliage types, cropland and forest.

The homogeneous cropland clutter scene of interest is shown in Figure 4. The aim point for this scene is 4.6 km northwest of the scene in Figure 3. The range from the aircraft to the physical domain of the image 4493 m, at a grazing angle of 15.14°. The scene is thoroughly homogeneous with the exception of the road in the extreme lower right corner. Only the homogeneous portion of the image is used in subsequent calculations.
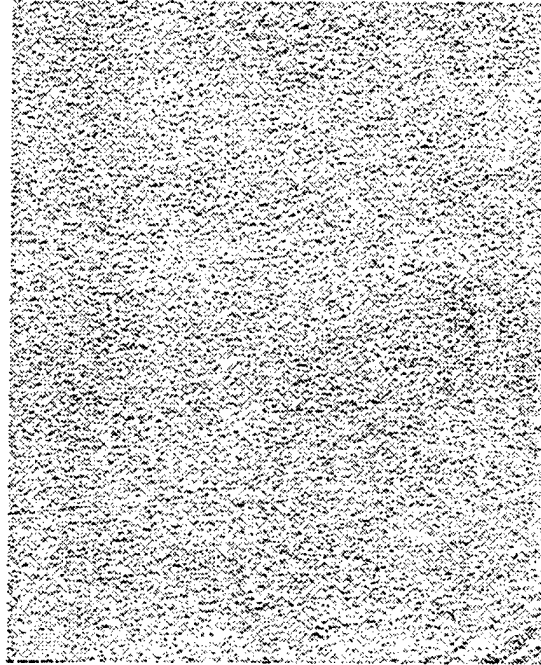

Figure 4. MSTAR Cropland Clutter Scene. Intensity image of cropland about an aim point located 4.6 km northwest of the scene in Figure 3, and viewed at a 15.14° grazing angle.
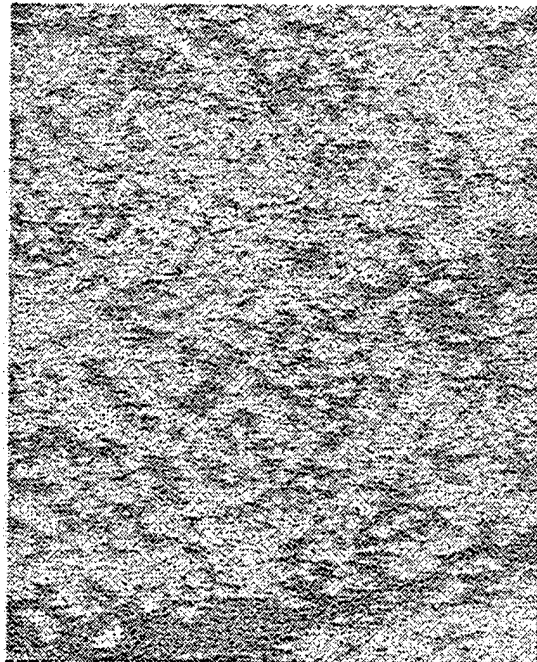
Figure 5. MSTAR Forest Clutter Scene. Intensity image of forested terrain about an aim point located 2.1 km northeast of the scene in Figure 3, and viewed at a 15.17° grazing angle.

Finally, Figure 5 shows the intensity image of the forest clutter scene used in this work. The aim point here is 2.1 km northeast of the scene in Figure 3. The range is 4492 m, and the grazing angle is 15.14°. Although the scene exhibits small scale inhomogeneity, it is uniformly forested and is characteristic of forest clutter throughout.

5. Clutter Pixel Statistics

In order to examine the statistical behavior of the clutter pixels, we need to select pixels whose signal values represent independent spatial realizations of the clutter return. A necessary, but not sufficient, condition for the independence of the pixel values is that they be uncorrelated. Even though uncorrelated random variables are not guaranteed to be independent, we will assume that pixels are independent if they are separated in space by more than the observed spatial decorrelation length of the pixel values.

The only alternative approach to establishing the independence of candidate pixels is to argue that the scatterers in the physical domain of the image are independent, independently located, and small relative to some number of pixels. Certainly, in the cropland and forest images under consideration the individual scatterers are plants or tree limbs that are physically independent and confined to meter-scale regions. However, it is not at all certain that their positions are independent. It is in fact reasonable to expect that

13

their positions are influenced by human or natural biological constraints. If we assume these constraints are local, then there will still be some distance beyond which the scatterer locations are independent. We will use the spatial decorrelation length as our guide to estimating that distance.

We determine the spatial decorrelation length by examining the autocovariance sequence of vectors of the complex pixel values along the range and cross-range dimensions of the image. The autocovariance sequence, $c_{xx}[m]$, of a complex vector x of length N is given by

$$c_{xx}[m] = \begin{cases} \sum_{n=0}^{N-|m|-1} \left(x_n - \frac{1}{N}\sum_{i=0}^{N-1} x_i \right)\left(x_{n+m}^* - \frac{1}{N}\sum_{i=0}^{N-1} x_i^* \right); & m \geq 0 \\ c_{xx}^*[-m]; & m < 0 \end{cases} \qquad (15)$$

Figure 6 plots several estimates of $|c_{xx}[m]/c_{xx}[m=0]|$ for $m > 0$, where the normalization ensures that the autocovariance at lag m = 0 is identically 1. The estimates shown are obtained by element-wise averaging the normalized autocovariance sequences for seven rows or columns in the pixel array.
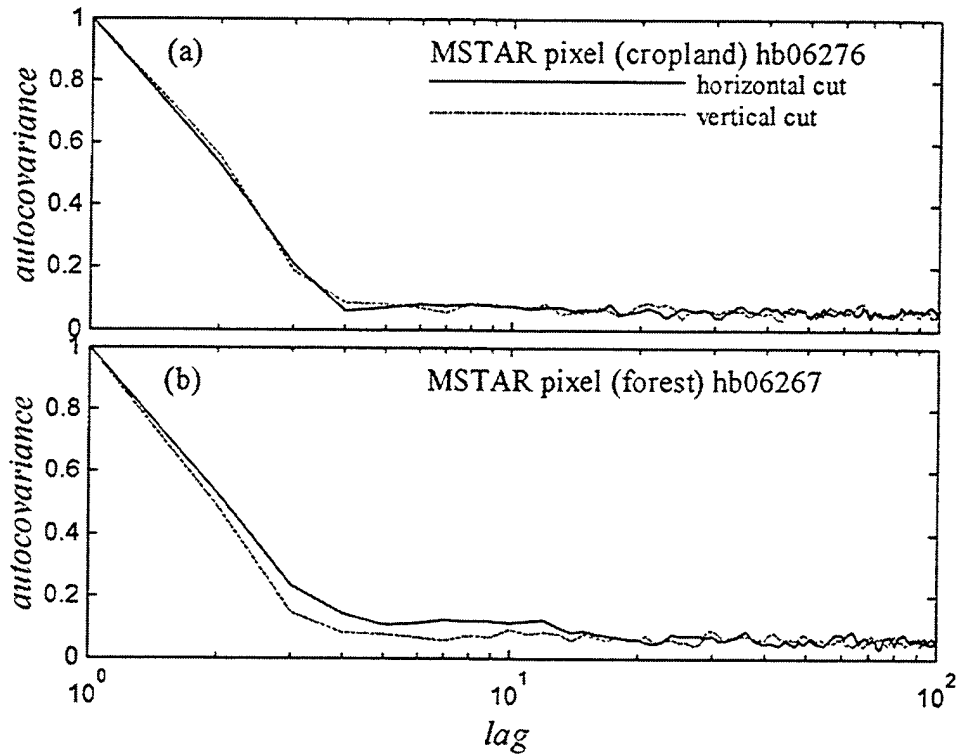

Figure 6. Normalized Spatial Correlation Of Clutter Pixels. Magnitude of autocovariance of complex pixel voltage values, normalized to 1 at zero lag for (a) cropland scene, (b) forest scene. Plotted curves show element-wise averages of normalized autocovariance along 10 separate horizontal (solid) or vertical (dashed) cuts through image.

14

The figure demonstrates that the autocovariance drops to 10% or less of its peak value within a three pixel lag. This is true regardless of the direction of the cut through the image, and regardless of the terrain cover. The only manner in which any one of the cases is distinguished is that the horizontal cut through the forest image does show a slight plateau out to a lag of ten pixels before declining to its ultimate floor value. Nevertheless, in all cases it appears that we can obtain uncorrelated samples by skipping at least four pixels.

Thus, in order to cull a pool of independent realizations of the pixel values, we move through the array of pixels, skipping four pixels in each dimension as we go. We then form a histogram for the pool of real or imaginary components of pixel values. Equivalently, we can compute normalized clutter cross sections from the calibrated pixel values using Eq. (12) and form a histogram from them. In either case, the properly normalized histogram will provide an estimate of the probability density function of the random variable under consideration.

(a) MSTAR σ_C (dB) hb06276
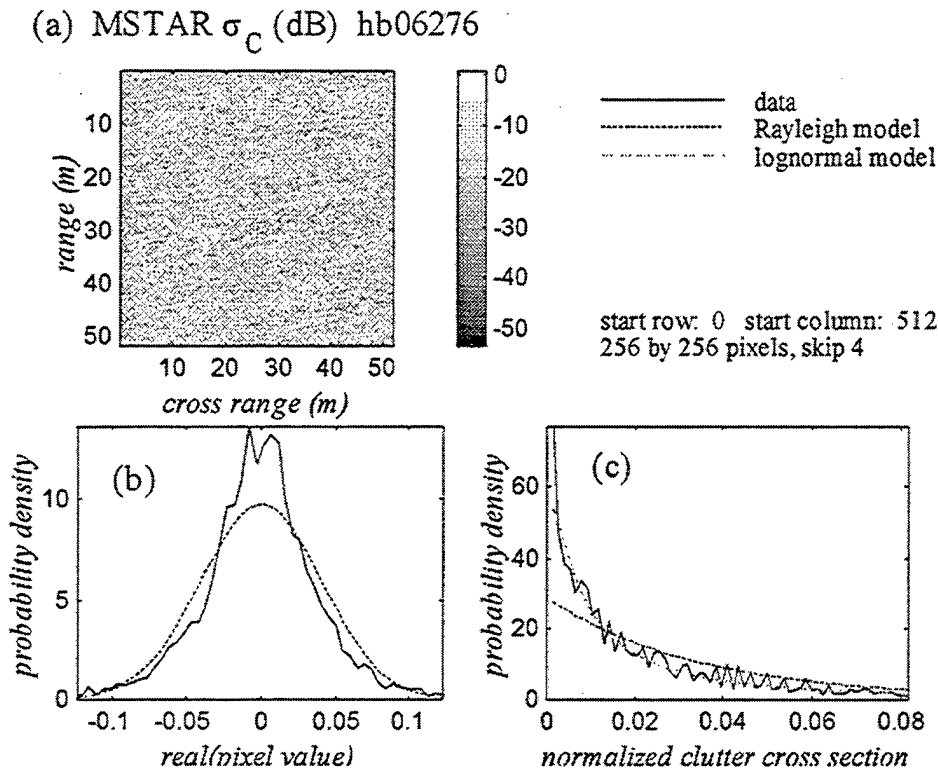
Figure 7. Statistics of Cropland Clutter Pixels. (a) Intensity image of pixels used in probability density function estimation. Image calibrated in normalized clutter cross section relative to 1 square meter. (b) Distribution of real part of pixel values, compared to model Gaussian distribution (Rayleigh clutter model) with variance equal to sample variance. (c) Distribution of normalized clutter cross section, compared to exponential (Rayleigh clutter model) and log-normal distributions with parameters estimated from sample.

15

Figure 7 compares the observed cropland pixel distribution with modeled Rayleigh and log-normal distributions. A total of 16,384 independent pixels were used to form the estimated distribution. The image formed by these pixels, in terms of calibrated, normalized clutter cross section is shown in Figure 7(a). Figure 7(b) compares the observed pdf for the real part of the pixel values (proportional to the I receiver voltage contribution of the associated resolution cells) with the Gaussian density that would be obtained for Rayleigh clutter. The model Gaussian uses a variance equal to the sample variance of the real part of the pixel values. The figure shows the pixel clutter to be non-Rayleigh, with the likelihood of extremely low and high values enhanced at the expense of moderate clutter values. The shoulders of the pdf are depleted.

Panel (c) compares the observed pdf for the normalized clutter cross section with both the Rayleigh and log-normal distributions. The mean used for the model exponential distribution (Rayleigh clutter model) is the sample mean of the observed distribution, 0.0349 or −14.6 dB. Reference 12 gives a value of −14.9 dB for σ_0 for both horizontal and vertical polarization for grass- and tree-covered terrain. [12] Reference 13 gives values in the range −15 to −20 dB for crop and vegetation-covered terrain.[13] The mean of the clutter distribution is by definition the value of σ_0, in this case the mean

normalized radar cross section of flat cropland clutter at 15° grazing angle. The parameters of the model log-normal distribution in Eq. (5) are also estimated from the sample.

The comparisons between the observed clutter pdf and the Rayleigh clutter model in Figure 7 panels (b) and (c) are equivalent. The comparisons illustrate two different functions of the same random variable. They both show poor agreement between the observed clutter and the Rayleigh model. On the other hand, the distribution of the observed clutter cross section agrees reasonably well with the log-normal model. We may quantify the quality of the agreement by appealing to the chi-square goodness-of-fit test.

The chi-square goodness-of-fit test is one of several means to assess whether the difference between an observed distribution and a model is statistically significant. For this purpose, we consider the total number of realizations contained in the histogram bin with index i to be a random variable, X_i. If the expected value of X_i is large enough (typically greater than 10), then X_i represents a sum whose statistical distribution may be approximated by the normal distribution according to the Central Limit Theorem.[7] We can fashion a test statistic, Q_{k-1}, from the values of all the bins in the histogram:

$$Q_{k-1} = \sum_{i=1}^{k} \frac{(X_i - np_i)^2}{np_i}, \tag{16}$$

[12] Ulaby, Fawwaz T., and Dobson, M. Craig "Handbook of Terrain Scattering Statistics for Terrain", Artech House, Norwood MA 1989

[13] Long, Maurice W. *radar Reflectivity of Land and Sea*, Lexington Books, Lexington, MA 1975

where np_i is the expected number of realizations in bin i according to the model distribution. It can be shown that if X_i is a normal random variable, then Q_{k-1} is a chi-square random variable with $k-1$ degrees of freedom.

We can form the following hypothesis. H_0: The numbers of outcomes X_1, X_2, ..., X_k, (the numbers of realizations in bins 1, 2, ... , k) are consistent with an underlying statistical distribution that has expected values np_1, np_2, ..., np_k, respectively. We reject H_0 if Q_{k-1} is too large, in particular, if $Q_{k-1} > q^*$. The value of q^* is chosen so that the chance of incorrectly rejecting H_0 is α, the significance level of the test. In practice, α is the area under the pdf of Q_{k-1} for which $Q_{k-1} > q^*$. Using this procedure we either accept or reject at significance α the hypothesis that an observed distribution is consistent with the model distribution.

Table 1 lists the chi-square statistics associated with the goodness-of-fit tests arising from Figure 7.

Table 1: Goodness of Fit Tests For Cropland (Figure 7)

Hypothesis	Chi-square statistic	Degrees of freedom
pixel amplitude is Rayleigh	257.3	39
clutter cross section is Rayleigh	675.3	58
clutter cross section is log-normal	55.9	58

The tests in the first two rows are equivalent, and they produce the same result, namely that we should reject the Rayleigh clutter model at any significance level. As a rule of thumb, the value of the chi-square statistic must be less than the number of degrees of freedom of the test in order to accept the hypothesis at even a low significance level. For the example of the test in the third row of Table 1, the greatest significance level at which we could accept the log-normal clutter hypothesis is 40%. This result suggests that the log-normal model provides a more reasonable fit to the observed cropland pixel statistics, and certainly a much better fit than the Rayleigh model. However, the agreement between the observed distribution and the log-normal model is not conclusive—as it might be if we could accept the hypothesis at a 99% significance level. Thus, computing the chi-square statistics for the several tests does not provide conclusive answers, but quantifies and confirms our visual assessment of the goodness of fit.
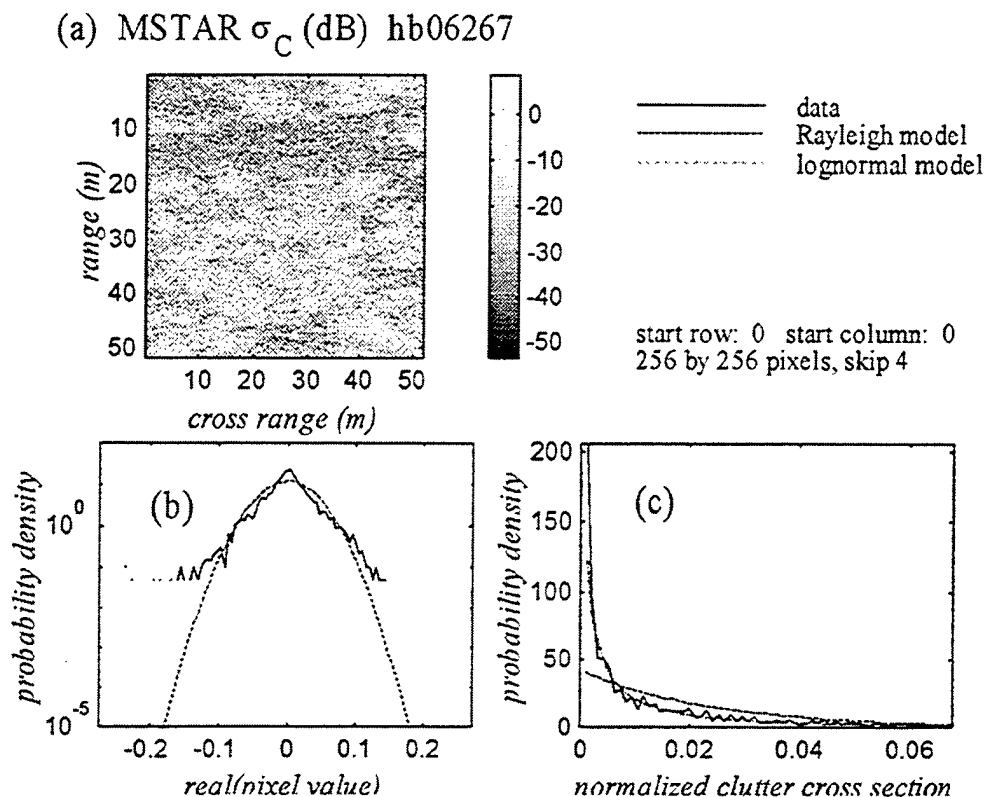
Figure 8. Statistics Of Forest Clutter Pixels. (a) Intensity image of the pixels used in probability density function estimation. Image calibrated in normalized clutter cross section per unit of ground clutter cell area. (b) Distribution of real part of pixel values, compared to model Gaussian distribution (Rayleigh clutter model) with variance equal to sample variance. Semilog plot illustrates high tails of observed distribution. (c) Distribution of normalized clutter cross section, compared to exponential (Rayleigh clutter model) and log-normal distributions with parameters estimated from sample.

For the forest data in Figure 8, $\sigma_o = -13.8\,dB$, in good agreement with the value reported in Reference 12 for tree-covered terrain. Figure 8 shows that neither the Rayleigh nor the log-normal model provides a reasonable fit to the observed pixel distribution, although the log-normal does the better job of the two. Figure 8(b) is a semilog plot that demonstrates that the observed amplitude distribution exhibits higher tails than the Rayleigh distribution. The chi-square statistics associated with Figure 8 are given in Table 2.

Table 2: Goodness of Fit Tests For Forest (Figure 8)

Hypothesis	Chi-square statistic	Degrees of freedom
pixel amplitude is Rayleigh	686.1	33
clutter cross section is Rayleigh	2411.0	47
clutter cross section is log-normal	318.0	47

Figures 7 and 8 suggest that while the log-normal distribution reasonably models cropland clutter pixel statistics, neither the log-normal nor the Rayleigh distribution is able to model the forest pixels. In order to assess whether these results are reproducible for other, similar clutter patches, we examine 10 non-overlapping 256 by 256 pixel sub-images within the clutter scenes of Figures 4 and 5. Figure 9 demonstrates that the observed distributions of the pixels in the different sub-images do overlay one another. The results are thus consistent among different examples of the same terrain cover. We may then meaningfully average the several instances of the observed pdf to obtain the mean pdf's shown in panel (c). The principal systematic difference between the cropland and forest pixel distributions is the greater likelihood of a low cross section for forest clutter than for cropland clutter. Probability density for the forest clutter cross section is heaped up at the lowest clutter values. This may be explained by the higher relief of the forest scene and the resulting greater degree of shadowing, which produces large areas of minimal radar return.

Table 3 shows the results of chi-square hypothesis tests for each of the cropland and forest sub-images. The results demonstrate strong non-Rayleigh statistical behavior for both cropland and forest terrain cover. The Rayleigh clutter model cannot be accepted, even at the weak 0.1 significance level, for any of the clutter sub-images. On the other hand, the log-normal distribution does reasonably model the cropland clutter pixel statistics. The log-normal hypothesis for cropland clutter can be accepted at the 0.5 significance level for 4 of 10 cases. Finally, neither the Rayleigh nor the log-normal model performs well for the forest clutter pixels.

We conclude that for both types of terrain cover examined here, the statistical distribution of clutter returns is non-Rayleigh for sufficiently small resolution cells (in this case 0.3 m by 0.3 m). We next turn to the question of how the distribution changes with the resolution cell size and shape.
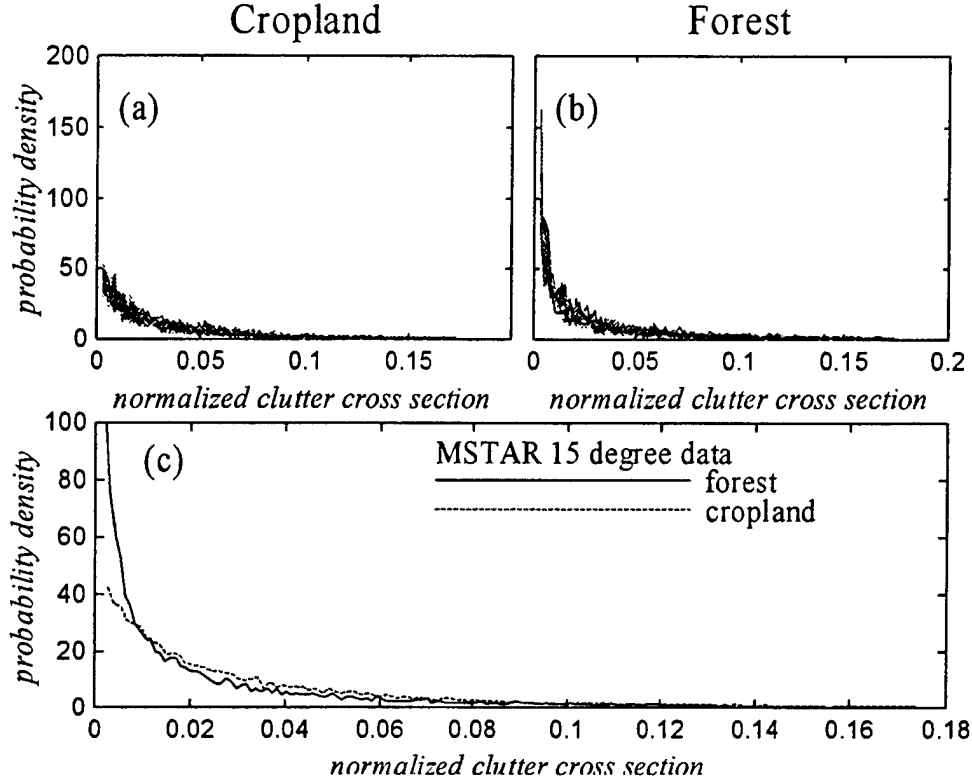
19

Figure 9. Clutter Cross Section Pixel Statistics. Observed distributions of normalized pixel cross section are estimated for 10 separate, non-overlapping sub-images taken from the cropland (Figure 4) and forest (Figure 5) clutter scenes. The resulting pdf estimates are plotted over one another for (a) the cropland scene and (b) the forest scene in order to demonstrate the consistency of the results. The 10 instances of each terrain cover type are averaged in (c).

Table 3 shows the results of chi-square hypothesis tests for each of the cropland and forest sub-images. The results demonstrate strong non-Rayleigh statistical behavior for both cropland and forest terrain cover. The Rayleigh clutter model cannot be accepted, even at the weak 0.1 significance level, for any of the clutter sub-images. On the other hand, the log-normal distribution does reasonably model the cropland clutter pixel statistics. The log-normal hypothesis for cropland clutter can be accepted at the 0.5 significance level for 4 of 10 cases. Finally, neither the Rayleigh nor the log-normal model performs well for the forest clutter pixels.

We conclude that for both types of terrain cover examined here, the statistical distribution of clutter returns is non-Rayleigh for sufficiently small resolution cells (in this case 0.3 m by 0.3 m). We next turn to the question of how the distribution changes with the resolution cell size and shape.

20

Table 3. Clutter Pixel Statistics Summary For Forest And Cropland

| Hypothesis | Cropland Cover | | | Forest Cover | |
	Rayleigh	Log-normal		Rayleigh	Log-normal
Significance	0.1	0.5	0.1	0.1	0.1
A sub-image	reject	ACCEPT	ACCEPT	Reject	Reject
B	reject	reject	ACCEPT	Reject	Reject
C	reject	ACCEPT	ACCEPT	Reject	Reject
D	reject	reject	Reject	Reject	Reject
E	reject	reject	Reject	Reject	Reject
F	reject	ACCEPT	ACCEPT	Reject	Reject
G	reject	reject	ACCEPT	Reject	Reject
H	reject	ACCEPT	ACCEPT	Reject	Reject
I	reject	reject	ACCEPT	Reject	Reject
J	reject	reject	Reject	Reject	Reject

6. Constructed Clutter Cell Statistics

In order to examine the statistical behavior of the clutter returns from resolution cells of various shapes and sizes, we coherently add the returns from the pixels which compose the constructed clutter cell, as described by Eq. (6). We will see that the probability density function of the clutter returns constructed in this way does vary systematically with both the size and the shape of the imagined clutter cells. We will consider only rectangular resolution cells. The naming conventions for the cell shapes is illustrated in Figure 10.
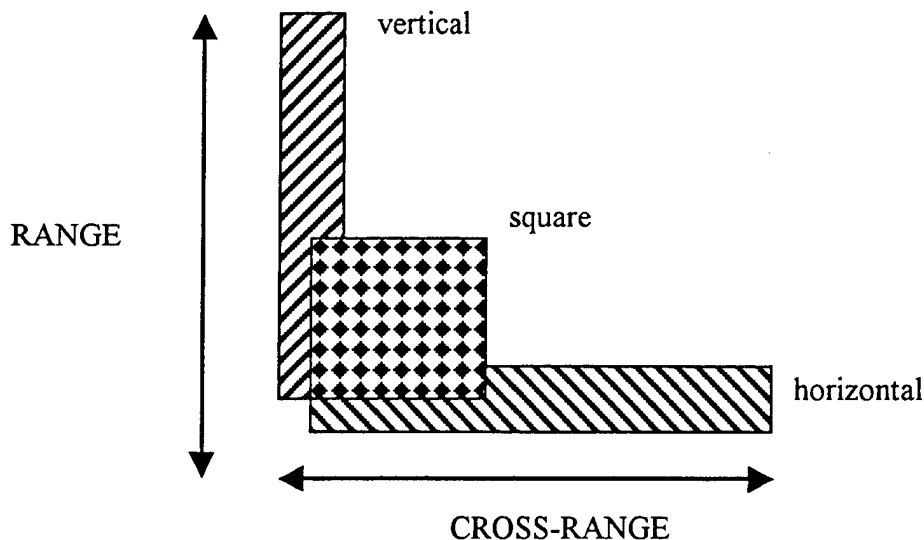
Figure 10. Naming Convention For Constructed Rectangular Clutter Cells. The terms vertical and horizontal derive from the clutter scene images frown in Figures 3 through 5. A vertical cell is long in the range dimension, while a horizontal cell is long in the cross-range dimension.

Just as in the case of our examination of the clutter pixel statistics, it is first necessary to make sure that the cells we include in our sample space are independent realizations of the same notional cell. We first obtain multiple realizations of equivalent clutter by dividing a homogeneous clutter scene into many equally sized sub-arrays of pixels. We then must ask whether all of these realizations are independent. The best we can do in this regard is to establish that they are at least uncorrelated, if not actually independent. To this end, we compute the autocovariance of clutter returns from representative 16 by 16 pixel clutter cells. The results are shown in Figure 11.

On the basis of Figure 11, it is evident that the array of constructed cells decorrelates from one cell to the next. The decorrelation in this case comes about much more rapidly than in the case of a pixel array because the mean spatial separation of the constructed cells is 16 pixels, and Figure 6 demonstrates that the pixels themselves decorrelate over a distance of several pixel dimensions. Thus, the clutter returns from adjacent constructed cells are uncorrelated, and we will take them to be independent as well.
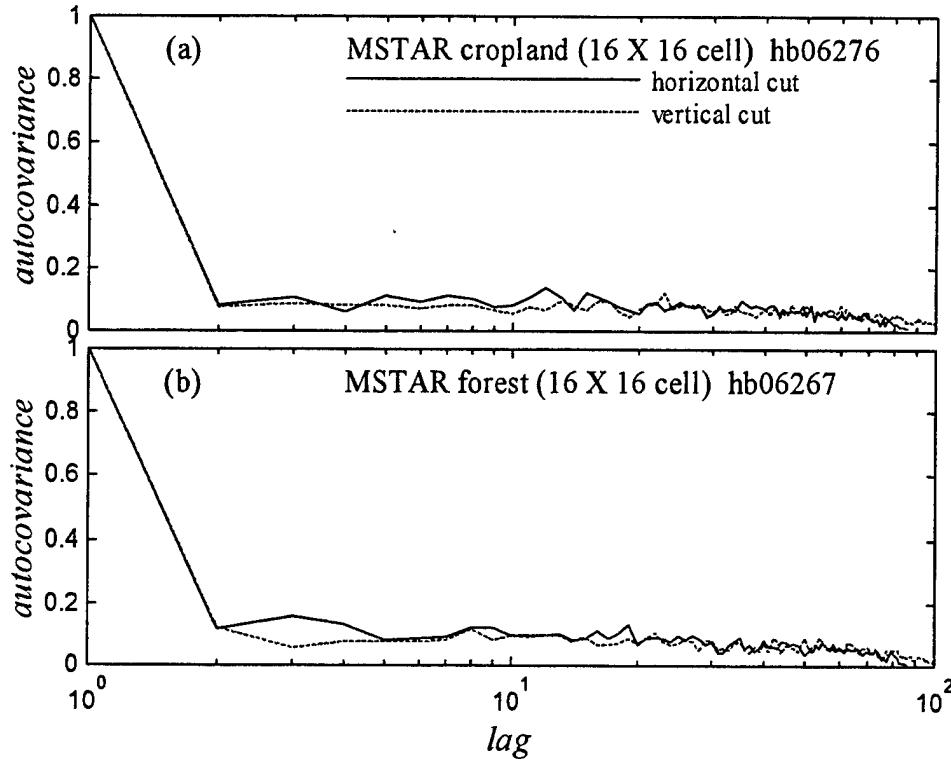
22

Figure 11. Normalized Spatial Correlation Of Returns From Constructed Clutter Cells Of Dimension 16 Pixels By 16 Pixels. Magnitude of autocovariance of complex cell values, normalized to 1 at zero lag for (a) cropland scene, (b) forest scene. Plotted curves show element-wise averages of normalized autocovariance along 10 separate horizontal (solid) or vertical (dashed) cuts through the array of cells.

As an example of the statistical behavior of clutter values for relatively large constructed resolution cells, Figure 12 shows the comparison between the Rayleigh clutter model and the estimated distribution of the real part of the cell values for cropland cells that are 0.6 m long in the range dimension and 77 m long in the cross-range dimension. This is an example of a horizontal clutter cell. According to the results of the associated chi-square test, we can accept at a 0.997 significance level the hypothesis that the estimated distribution is in truth a Gaussian, consistent with the Rayleigh clutter model.

It is straightforward to explain why the statistical distribution of a large clutter cell, formed as the sum of returns from a large number of pixels, is Gaussian. This result is a simple consequence of the Central Limit Theorem. We conclude that for a sufficiently large resolution cell and homogeneous clutter, the clutter will always be Rayleigh, as in the example of Figure 12. This is true regardless of the type of terrain cover. The open issue is the rate at which the clutter distribution approaches the Rayleigh model, as a function of cell size and parameterized by cell shape.

23

(a) MSTAR σ$_C$ (dB) hb06276

chi-square test
Rayleigh statistic = 40.249 degrees = 68

cell is 2 by 256pixels
start row: 0 start column: 0
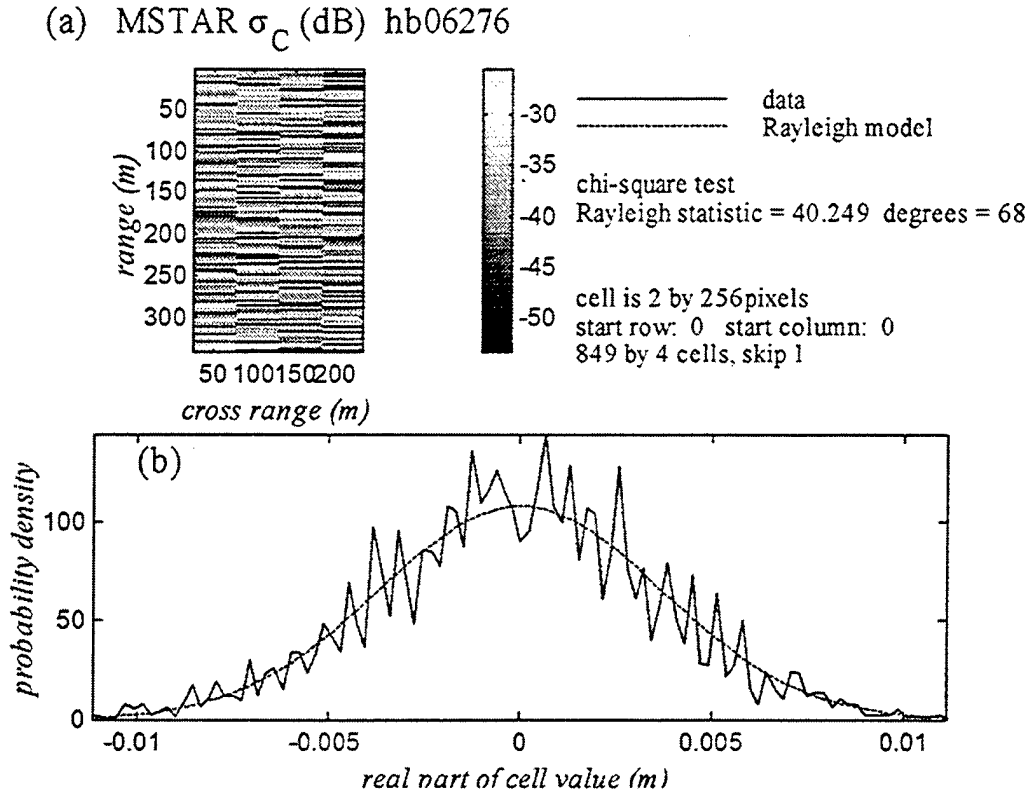849 by 4 cells, skip 1

Figure 12. Statistics of Constructed 0.6 m By 76.8 m Cropland Clutter Cells. (a) Intensity image of constructed clutter cells used in probability density function estimation. Image calibrated in normalized clutter cross section relative to 1 square meter. (b) Distribution of real part of cell values, compared to model Gaussian distribution (Rayleigh clutter model) with variance equal to sample variance.

It is natural to quantify the approach of the observed clutter distributions to Rayleigh in terms of the chi-square statistic characterizing the fit of the Rayleigh hypothesis to each observed distribution. We can divide the cropland and forest clutter scenes into ensembles of horizontal, vertical, or square cells of various sizes. For example, we can form separate ensembles of horizontal cells with dimensions of 2 by 4, 2 by 8, 2 by 16, 2 by 32, 2 by 64, and so forth. For the observed sample space associated with each cell size, we can perform the analysis indicated in Figure 12 to compute the chi-square statistic for a fit to the Rayleigh model. The results of many such analyses are shown in Figure 13.
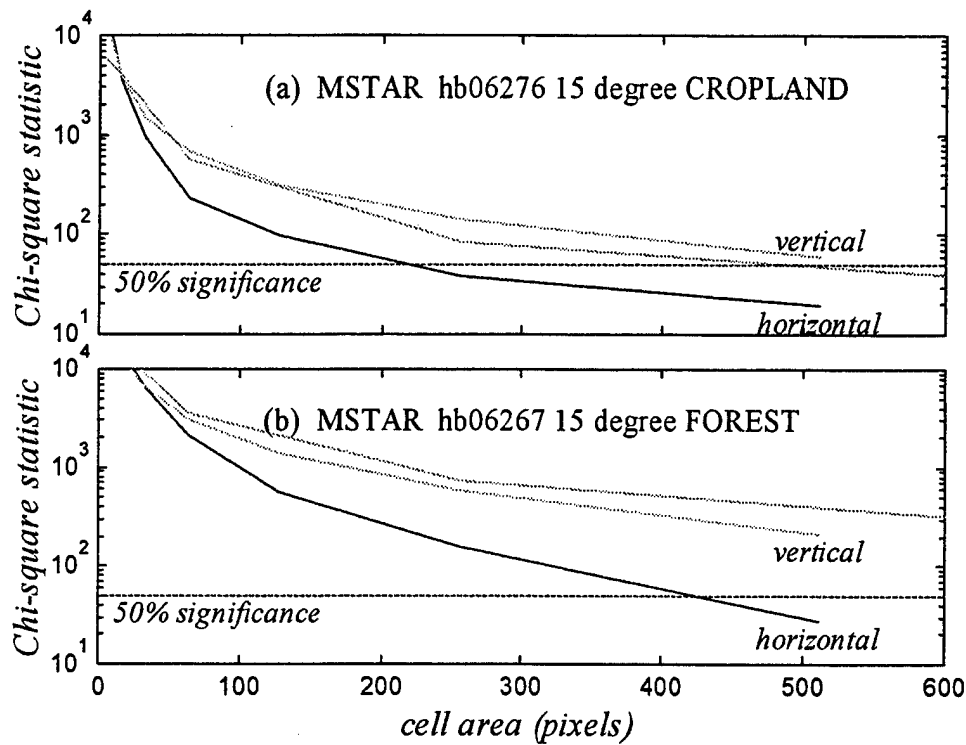
Figure 13. Shape And Size Dependence Of Constructed Clutter Cell Statistical Distribution. Chi-square statistic for fit of observed clutter distributions to Rayleigh model. Fit improves for decreasing value of test statistic at roughly constant number of degrees of freedom (approximately 50). Vertical, square (unlabeled), and horizontal cell shapes are compared for (a) cropland and (b) forest terrain cover. Dashed line shows value of statistic below which the Rayleigh model can be accepted at a 0.5 significance level.

In Figure 13 we record the chi-square statistic for the discrepancy between the Rayleigh model and the distribution observed for each resolution cell size and shape. A value much greater than the number of degrees of freedom in the test means that the Rayleigh hypothesis cannot be accepted, while values much less than the number of degrees of freedom indicate that the observed distribution is fully consistent with the Rayleigh model.

Two points are clear from Figure 13. First, regardless of the type of terrain cover, the horizontal cells approach the Rayleigh clutter model much more quickly with cell size than do either the square or the vertical cells. Second, regardless of the cell shape, cropland clutter approaches Rayleigh more quickly with increasing cell size than does forest clutter. Both of these effects are the result of shadowing.

We pointed out in connection with Figure 3 that the radar platform was located beyond the bottom of each image, so that the radar shadows extend upward in the range (vertical) dimension. Clearly, in the presence of shadowing, the pixel values are not independent in the vertical direction. An elevated reflector in one pixel can lead to a high

amplitude return in that pixel while its shadow leads to a low return in the pixels immediately behind it (or vertically above it in the clutter scene image). This effect will be stronger for clutter cells that are long in the range dimension, and will disappear for cells that are very narrow in range and long in cross-range. In effect, shadowing requires us to take a longer vertical cell than horizontal cell to obtain enough independent contributions to satisfy the Central Limit Theorem.

Similarly, the forest clutter scene exhibits greater relief and greater shadowing than the cropland scene. Thus, for each cell shape, the forested terrain requires a larger cell area to obtain enough independent realizations of the clutter to achieve the Rayleigh model. This is precisely the result demonstrated by comparing Figure 13 panel (a) and panel (b).

Since shadowing is more pronounced at lower grazing angles, we should expect that its effects on the clutter distribution will be stronger in the 15° grazing angle case examined so far than at the alternative grazing angle of 45°. This prediction is borne out by Figure 14, which compares the approach to Rayleigh of clutter in vertical cells from the same scene, observed at 15° and 45°. The test area is different from that cited in Figure 13. No conclusion should be drawn from the difference in the test statistics in Figures 13 and 14, since the χ^2 statistic varies widely with the particular model and samples, especially when actual statistics are far from the test model. While the data for neither grazing angle actually achieves a good fit to the Rayleigh model, the 45° case does approach Rayleigh faster. This is consistent with the role of shadowing in destroying the independence of pixel clutter returns in the range direction.
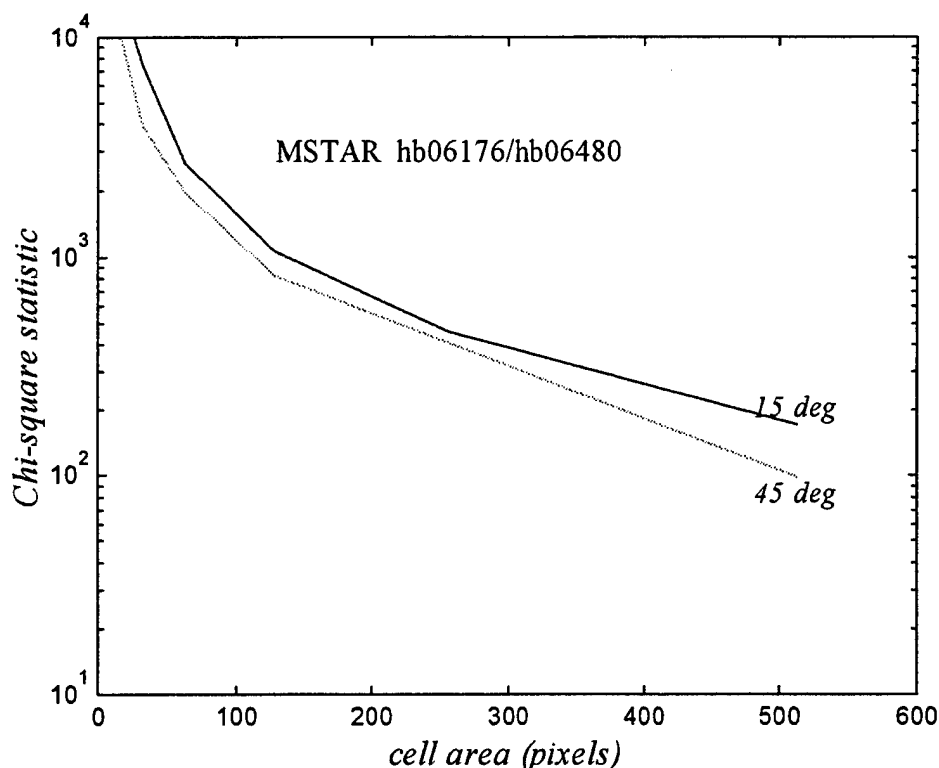
Figure 14. Dependence Of Clutter Statistical Distribution On Grazing Angle For Constructed Vertical Cells. Chi-square statistic indicates goodness of fit of model Gaussian (Rayleigh clutter) to observed distribution of clutter cell values. Downward sloping curves indicate approach of observed clutter to Rayleigh as cell area increases. Approach to Rayleigh is faster at 45° grazing angle than at 15°.

7. Conclusions

We present a straightforward technique for estimating the statistical distribution of clutter returns from resolution cells of arbitrary size and shape. The technique is based upon the coherent addition of high resolution clutter measurements made using a synthetic aperture radar. The principal conditions for this approach to be valid are:

1. The SAR imaging time must be short compared to the temporal decorrelation interval of the clutter that is imaged.
2. The angular diversity of the SAR measurements must be small compared to the aspect angle dependence of the clutter scene.
3. The clutter returns must not vary with frequency over the varying simulated bandwidths of the constructed clutter cells.

These conditions are met for the MSTAR data utilized in this report.

27

We show that the statistical distribution of individual pixel returns are distinctly non-Rayleigh—at odds with some predictions. In fact, the log-normal distribution provides an acceptable model of the distribution of cropland clutter pixels. For the other type of terrain cover considered, forest, neither the Rayleigh nor the log-normal models provide an acceptable fit to observation.

Rectangular clutter cells of various sizes and shapes can be constructed from the clutter pixels that compose the MSTAR clutter scene images. For all shapes and both terrain cover types considered, the statistical behavior of the clutter returns approaches the Rayleigh model as cell area increased. The analysis demonstrates notable differences in the rate at which the statistics approach Rayleigh, depending upon the cell shape and cover type. The approach is faster for cropland clutter than for forest, and faster for cells that are long in the cross-range dimension than for cells long in range. In other words, for resolution cells of equal area, the cell containing cropland clutter, or the one that is longer in cross range, will be better approximated by the Rayleigh clutter model.

The variation of clutter distribution with cell shape and terrain cover is attributed to the effects of radar shadows, which are more pronounced in the range dimension and in cases of high relief. Shadowing becomes less important at higher grazing angles, and data for 45° grazing angle do indeed show a more rapid approach to the Rayleigh model than do data for 15°.

Figure 15 demonstrates the operational significance of the statistical distribution of clutter returns. The figure compares the probability density functions of the clutter cross sections of cells with the same foliage cover (forest) and the same area (10 m^2), but different shape. The distribution of the cross sections for the square cells has a much higher tail than that for the horizontal cells, which are much longer in the cross-range dimension. In circumstances where the radar system is clutter limited, meaning that the clutter level exceeds the noise floor, the higher tail translates directly into a higher detection threshold. If we apply a Neyman-Pearson target detection criterion[14], the probability of false alarm determines the detection threshold. P_f is taken to be 0.005 in both cases—an unrealistically high value chosen for illustrative purposes. The resulting detection threshold for square cells is 10 dB higher than for horizontal cells. Thus, a cell that is long in cross-range allows detection of 10 dB smaller targets than does a square cell.

[14] Couch, L. W. II, (1987), *Digital and Analog Communication Systems, 2nd ed.*, Macmillan, New York, 551.
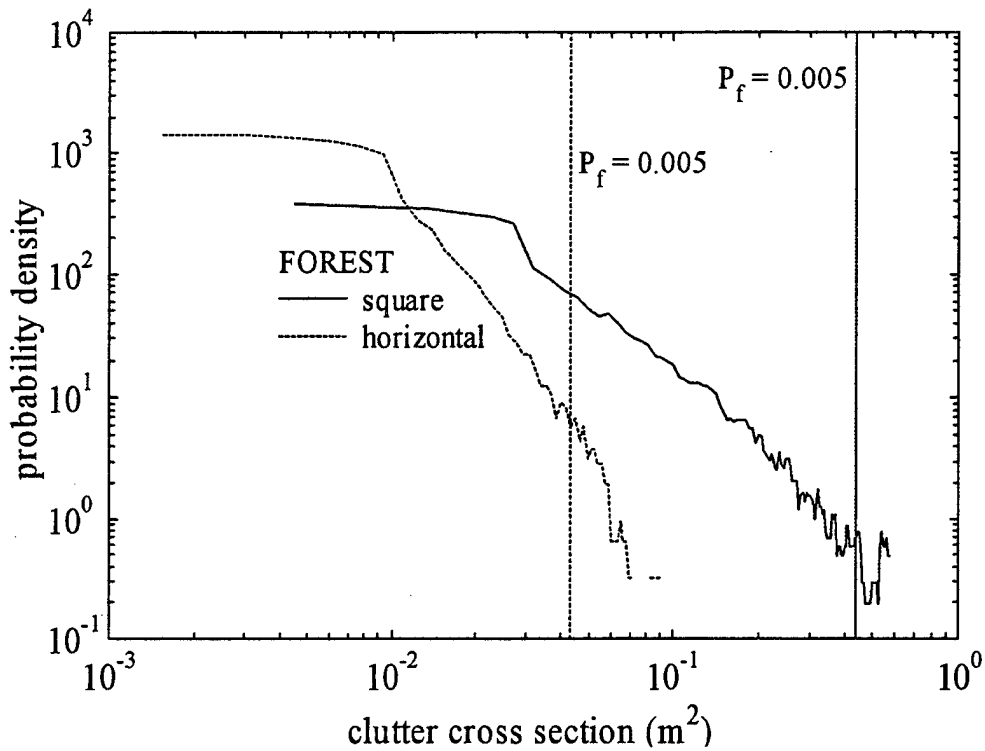
Figure 15. Cell Shape Effects On Detection Probability. Probability density functions are plotted for two differently shaped resolution cells, square and horizontal (rectangle long in cross-range). Both cases represent the same terrain cover and resolution cell area. The vertical lines represent detection thresholds set for 0.005 probability of false alarm using the Neyman-Pearson criterion. Threshold is 10 dB higher for the case of horizontal cells.

Figure 15 is a concrete example of the effects of resolution cell shape on detection probability and radar signal processing design. The technique of constructing statistical distributions for arbitrary cell shapes using SAR data enables us to examine the system consequences of the exotic resolution cell shapes that are encountered for proposed distributed aperture radars.

References

1. Skolnik, M. I. (1980) *Introduction to Radar Systems, 2nd ed.*, McGraw-Hill, New York, pp. 485-496.

2. TechSat 21, Sparse Array Workshop, Air Force Reasearch Laboratory, Space Vehicles Directorate, Kirtland AFB, NM, 28-29 July 1998

3. MSTAR (Public) Clutter, Web: http://www.mvblab.wpath.af.mil/public/MBVDATA; E-mail: cdhelp@mvblab.wpafb.af.mil; FAX: 937-656-4412

4. Ulaby, F. T., Moore, R. K., and Fung, A. K. (1986) *Microwave Remote Sensing, Active and Passive, Volume II*, Artech House, Norwood, MA, 903.

5. Fung, Adrian K., (1990) *Effect Of Cell Size On Radar Clutter Statistics*, University of Texas at Arlington, RADC Tech. Rpt. RADC-TR-90-235

6. Andrews, G. A. and Gerlach, K. (1989), "SBR Clutter and Interference", in *Space-Based Radar Handbook*, L.J. Cantafio, ed., Artech House, Norwood, MA, 388.

7. Papoulis, A. (1965) *Probability, Random Variables, and Stochastic Processes*, McGraw-Hill, New York, 250-266.

8. Skinner, J. Paul, Kent, Brian M., Wittman, Ronald C., Mensa, Dean L. and Andersh, Dennis J. "Normalization and Interpretation of Radar Images, IEEE Tran. AP VOL. 46, No. 4, April 1998

9. Jakowatz, C. V., Wahl, D. E., Eichel, P. H., Ghiglia, D. C., and Thompson, P. A. (1996) Spotlight-Mode Synthetic Aperture Radar: A Signal Processing Approach, Kluwer Academic Publishers, Boston, 107-109.

10. Curlander, J. C. and McDonough, R. N.(1991) Synthetic Aperture Radar: Systems and Signal Processing, John Wiley & Sons, New York, 215.

11. Skolnik, M. I. (1980) *Introduction to Radar Systems, 2nd ed.*, McGraw-Hill, New York, 40.

12. Ulaby, Fawwaz T., and //sobson, M. Craig "Handbook of Terrain Scattering Statistics for Terrain", Artech House, Norwood MA 1989

13. Long, Maurice W. *radar Reflectivity of Land and Sea*, Lexington Books, Lexington, MA 1975

14. Couch, L. W. II, (1987), *Digital and Analog Communication Systems, 2nd ed.*, Macmillan, New York, 551.